HELICOPTER ENGINE AIR INTAKE ICING WIND TUNNEL CERTIFICATION TEST

Karel Lammers, Karel.Lammers@nlr.nl, Netherlands Aerospace Centre NLR (The Netherlands)
Stefan van 't Hoff, Stefan.van.t.Hoff@nlr.nl, Netherlands Aerospace Centre NLR (The Netherlands)
Hermann Ferschitz, Hermann.Ferschitz@rta.eu, RTA Climatic Wind Tunnel Vienna (Austria)
Michael Wannemacher, Michael.Wannemacher@rta.eu, RTA Climatic Wind Tunnel Vienna (Austria)

Abstract
Korea Aerospace Industries LTD (KAI) contracted the Netherlands Aerospace Centre (NLR) to support an Icing Wind Tunnel (IWT) test campaign with the Korean Utility Helicopter KUH-1 engine air intakes aimed at substantiating the compliance with the applicable military regulations for flight in icing conditions. The icing wind tunnel test was performed in the Large Climatic Wind Tunnel (CWT) at Rail Tec Arsenal (RTA) in Vienna, Austria. The test set-up included a full-scale production engine cowling complete with electrothermal anti-icing system and it was installed on a mock-up of the aircraft upper fuselage. The production cowling was used to ensure an exact match and conformity of the thermal properties of the part. To aspirate the engine intakes, NLR designed a dedicated Engine Mass Flow System (EMFS) that simulates the airflow through the engine air and cooling intakes. Two separate industrial radial fans were installed to individually control the mass flow through the engine air intakes and cooling inlets. A continuous mass flow measurement was provided for both channels by anti-iced Pitot-static probes that were calibrated against orifice plate measurements performed prior to the icing test. The tunnel test conditions were scaled for altitude effects by matching key similarity parameters. The test airspeed was based on either Reynolds number scaling or Weber number scaling, depending primarily on the static air temperature. Inter-laminate and surface temperature measurements and observed ice shapes compared favourably with artificial and natural icing flight test results obtained with the same intake configuration. The IWT testing supplemented the flight test results by providing more stable icing conditions with control over drop size, and covering the corner points of the icing envelope.

1. INTRODUCTION

The Netherlands Aerospace Centre (NLR) has collaborated closely with Korea Aerospace Industries LTD (KAI) in the military qualification of the Korean Utility Helicopter KUH-1 for flight in icing conditions since the first icing flight trials performed in the winter of 2015/2016 [1]. The KUH-1 has been developed by KAI, with technical support from Airbus Helicopters, and is now in the final stages of achieving icing qualification. Following the first icing flight trials, KAI introduced a number of design improvements on the engine intake anti-icing system including an increase in the protected area and a redistribution of the power density. In parallel with a second icing flight test campaign, KAI and NLR performed a dedicated icing wind tunnel (IWT) test campaign at Rail Tec Arsenal (RTA) in Vienna, Austria, in March 2018, to enable the system performance to be substantiated in all corner of the certification icing envelope. The test marks the second and final tunnel entry for the intake ice protection system after initial testing at CIRA in 2012 [2]. This paper presents an overview of the wind tunnel model, including the new Engine Mass Flow Simulator (EMFS), the test facility, and the test activities themselves.

2. WIND TUNNEL MODEL

2.1. Helicopter mock-up

The full-scale intake model is comprised of two main parts, the KUH-1 mock-up and the EMFS, see Figure 1.

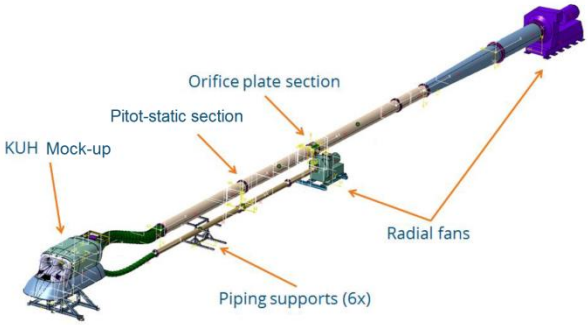

Figure 1: Full-scale intake model as used during the intake IWT of the KUH-1 at RTA. Total length is approximately 32 meters.

The shorter flow channel with the smaller radial fan is connected to both engine cooling inlets, and the larger flow channel with the larger fan is connected to both main engine air inlets. In this way, the mass flow through both sets of inlets can be controlled separately. Both flow channels follow the same design approach. The KUH-1

Presented at 44th European Rotorcraft Forum, Delft, The Netherlands, 19-20 September, 2018

wind tunnel model consists out of a rigid metal frame and fiber glass shell structure that represents the helicopter geometry surrounding the intake, see Figure 2. A production intake cowling including a 9.3 kW electrothermal ice protection system was installed on the mock-up. During the IWT test, two interchangeable intake cowlings were available with different ice protection power density distributions. The support frame allows for ±5° Angle of Attack (AoA) and ±2° Angle of Sideslip (AoS) adjustment as may be required to simulate different flight conditions.

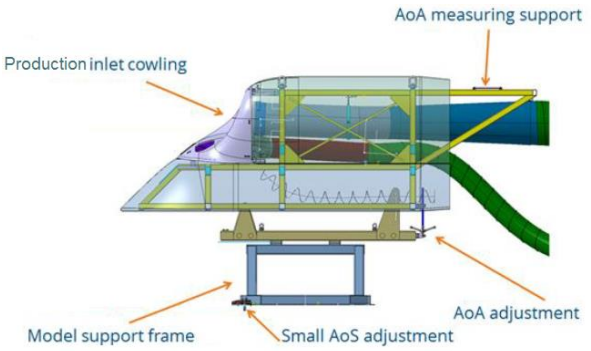

Figure 2: KUH-1 wind tunnel model including production intake cowling.

2.2. Engine Mass Flow Simulator (EMFS)

Each flow channel of the EMFS includes a rigid stainless steel pipe section and a flexible interface to the model that accommodates thermal expansion/contraction of the steel parts and allows for the aforementioned AoA and AoS adjustments.

Downstream of the flexible interface, the long and straight steel pipes include an anti-iced Pitot-static section and an orifice plate section. The Pitot-static and orifice plate sections are interchangeable and separated by a straight pipe of sufficient length to attenuate any flow distortions in between the measurement stations. Downstream of the Pitot-static tube and orifice plate there is another straight length of pipe to ensure reasonably uniform flow at the entrance of the radial fans. For the larger flow channel an additional diffusor is necessary to connect to the larger diameter fan inlet flange. The length of the diffusor is such that no flow separation occurs. The pipes of the EMFS are supported by frames that allow streamwise repositioning of the pipes/fans, as well as some vertical adjustment to set a non-zero slope for drainage purposes.

Both channels are equipped with an exchangeable anti-iced Pitot-static tube that provides the calibrated mass measurement. The Pitot-static tube is located at the centerline of the flow channel in a fully developed pipe flow with approximately uniform velocity distribution over the cross-section. An inverted PT100 total temperature sensor is installed on the downstream side of the Pitot-static tube mount to measure the local static air temperature.

Prior to the IWT test a calibration was performed to determine the relation between the average velocity in the pipe and the point measurement of the Pitot-static tube in the fully developed turbulent pipe flow radial velocity profile, see Figure 3.

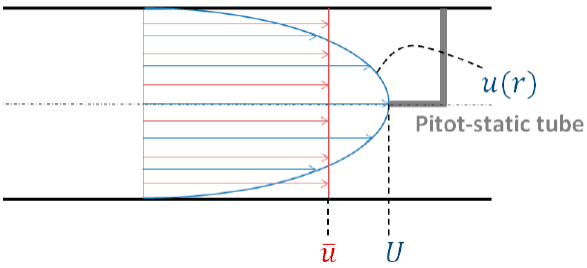

Figure 3: Schematic velocity profile at the Pitot-static tube.

With help of isentropic relationships, the local Mach number (at location of the Pitot-static tube) can be determined from:

$$\frac{p}{p_t} = \left(1 + \frac{\gamma - 1}{2} M^2\right)^{\frac{-\gamma}{\gamma - 1}} \quad (1)$$

where p is the static pressure, p_t is the total pressure, γ is the specific heat ratio and M is the Mach number.

The local axial velocity on the centerline of the pipe, U, is then given by the Mach number multiplied by the speed of sound, a:

$$a = \sqrt{\gamma R T} \quad (2)$$

where T is the static temperature and R is the gas constant.

The pipe mass flow, $\dot{m}$, is given as:

$$\dot{m} = \rho \bar{u} A = \rho C U A \quad (3)$$

where $\bar{u}$ is the average axial velocity, ρ is the density, A is the area of the cross-section of the pipe, and C is a calibration coefficient. During the calibration, the mass flow was determined from the pressure loss over the orifice plate according to the relations defined in ISO 5167-1 [3]. The density is calculated via the ideal gas law, with the measured static pressure and static air temperature as input. This enables the calculation of the calibration coefficient $C = \bar{u}/U$. It is shown

Presented at 44th European Rotorcraft Forum, Delft, The Netherlands, 19-20 September, 2018

below that the calibration coefficient is largely independent of air temperature. This means that the same value coefficient can be used for all test points in the test matrix and the calibration can be performed at room temperature outside of the test section.

According to the boundary layer theory of Schlichting et al. [4], the dimensionless coefficient of friction for pipe flow, λ, is given by the empirical relation of equation (4).

$$\frac{1}{\sqrt{\lambda}} = 2\log\left(\mathrm{Re}\sqrt{\lambda}\right) - 0.8 \tag{4}$$

where Re is the Reynolds number.

A useful quantity in boundary layer theory is the friction velocity, v_*. This quantity is used to express the shear stress at a surface (e.g., a wall) in terms of velocity. The friction velocity in terms λ is given by Schlichting as:

$$v_* = \bar{u}\sqrt{\frac{\lambda}{8}} \tag{5}$$

According to Schlichting, the centerline velocity U for hydraulically smooth pipes is then:

$$U = \bar{u} + 4.07v_* \tag{6}$$

To show the negligible effect of air temperature on the velocity profile, Table 1 and Table 2 present the results calculated at +20°C and at -30°C static air temperature for the large and small flow channel, respectively. It can be seen that the velocity profile as characterized by $\bar{u}/U$ is not significantly affected.

The error due to the assumption that the velocity profile is not affected by air temperature can be computed as:

$$E = \frac{\left(\frac{\bar{u}}{U}\right)_{-30} * U_{-30} * \rho_{-30} * A - \left(\frac{\bar{u}}{U}\right)_{+20} * U_{-30} * \rho_{-30} * A}{\left(\frac{\bar{u}}{U}\right)_{-30} * U_{-30} * \rho_{-30} * A} = 1 - \frac{\left(\frac{\bar{u}}{U}\right)_{+20}}{\left(\frac{\bar{u}}{U}\right)_{-30}} \tag{7}$$

Equation (7) yields a mass flow error of 0.16% for the large flow channel due to temperature effects, and an error of 0.20% for the smaller flow channel.

The equations above assume hydraulically smooth pipes. This assumption is generally valid when $0 \leq \frac{kv_*}{\nu} \leq \sim 5$. The calculations in Table 1 show that the large flow channel is near the upper limit of this range at +20°C. However, the experimental data in Figure 4 shows that, with an expected manufacturing roughness of $R_p/k = 7500$ (where R_p is the radius of the large flow channel) and a Reynolds number of 8.4×10^5, the large flow channel can indeed be considered hydraulically smooth.

Table 1: Large inlet flow channel velocity profile parameters for different air temperatures at fixed mass flow.

OAT [°C]	Re x10^5	ū [m/s]	ρ/ρ_0	λ x10^{-3}	v_* [m/s]	U [m/s]	$\bar{u}/U$	kv_*/ν
+20	8.44	57.0	0.97	1.20	2.21	66.0	.864	6.1
-30	9.73	47.2	1.18	1.17	1.80	54.5	.865	5.0

Table 2: Small inlet flow channel velocity profile parameters for different air temperatures at fixed mass flow.

OAT [°C]	Re x10^5	ū [m/s]	ρ/ρ_0	λ x10^{-3}	v_* [m/s]	U [m/s]	$\bar{u}/U$	kv_*/ν
+20	1.62	44.1	0.97	1.50	1.62	44.1	.850	4.5
-30	1.33	36.4	1.18	1.46	1.33	36.4	.852	3.7

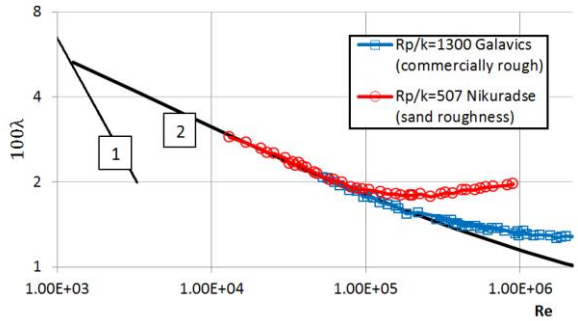

Figure 4: Resitance formula for rough pipes as presented by Schlichting et al. [4]. Experimental data from Bauer and Galavics [6] (red circles) and Nikuradse [7] (blue squares). Solid line 1 is applicable for laminar flow and solide line 2 is for turbulent flow in smooth pipes.

In theory, equation (4) can be used to correct for temperature effects. Schlichting et al. also derived expressions for non-hydraulically smooth pipes. However, given the small error introduced it was decided to maintain a constant calibration coefficient.

After completion of the Pitot-static tube calibration, the orifice plates were removed to leave a smooth transition between pipe segments that would not be subject to ice accretion.

2.3. Remote control & instrumentation

The production intake cowling is equipped with an electrothermal anti-icing system. The controllers were located close to the control room for operator control and monitoring purposes. The controller Voltage and current was recorded and displayed in real-time. The EMFS was controlled

Presented at 44th European Rotorcraft Forum, Delft, The Netherlands, 19-20 September, 2018

by manual dial input to frequency convertors to adjust the speed of the radial fans that provided the aspiration. The Pitot-static pressure and temperature data was recorded, and the calibrated intake mass flows were displayed in the control room. An emergency stop button was available to cut-off the power to the radial fans.

The intake ice protection system was equipped with 30 interlaminate Resistance Temperature Detectors (RTDs) and 30 surface thermocouples. A number of the thermocouples were later removed because of issues with local ice accretions on the wiring and relatively poor adhesion of the sensors to the rubber heater surface.

Remote control infrared and high-definition camera coverage was available throughout the test. After each test point, accreted ice was photographed, the dimensions measured, and subsequently removed to document the potential engine ingestion ice mass where relevant. For a selected set of test points, 3D scans of ice shapes were made by the Austrian Institute for Icing Sciences (AIIS).

3. TEST FACILITY

3.1. Large Climatic Wind Tunnel / Icing Wind Tunnel

The IWT test was performed at the Rail Tec Arsenal (RTA) in Vienna. RTA is a non-profit research organization. As an accredited testing laboratory, RTA provides its services completely impartially and independently and grants all its customers the same terms and conditions. The official accreditation according EN ISO/IEC 17025 requires strict compliance with stringent quality guidelines in terms of the correctness and reliability of the tests performed. RTA meets these high requirements by constantly improving the quality management system and by continuously upgrading the testing and measuring facilities in line with the latest developments in technology. RTA operates two Climatic Wind Tunnels. The large Climatic Wind Tunnel (large CWT), as shown in Figure 5**,** can be used for rail vehicles, road vehicles, technical systems, cold starting tests on aircraft engines and complete helicopters, air conditioning of cockpits, as well as for component testing under extreme temperatures, solar radiation and snow impact. Additionally, it can be used as an IWT.

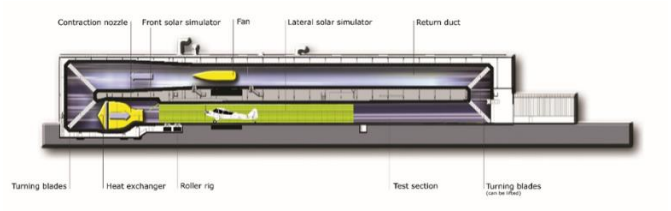

Figure 5: Large Climatic Wind Tunnel.

To adapt the large CWT to an IWT, a spray bar system is installed consisting of eleven spray bars, each equipped with 24 atomizing nozzles, i.e., 264 nozzles in total, see Figure 6. The spray bar system can be used with and without additional contraction nozzle, see Figure 7. For the KUH-1 engine intake tests, the configuration with additional contraction nozzle was used to be able to speed up to 80 m/s and to increase the maximum achievable Liquid Water Content (LWC) at the test section. Each of the spray bars features two independent circuits for water and air. The separate control for every second spray nozzle enables operation with only half of the nozzles for very low LWC test points, or other operations as necessary, e.g., for the generation of Supercooled Large Drops (SLD). The control of the spray LWC and Median Volume Diameter (MVD) is achieved by adjusting the water and air pressure for each circuit. Furthermore, the water and air supply temperature can be controlled separately in each circuit (cold and hot) to ensure the drops are supercooled, but not frozen when reaching the test section.

Figure 6: Spray bar system with atomizing nozzles.

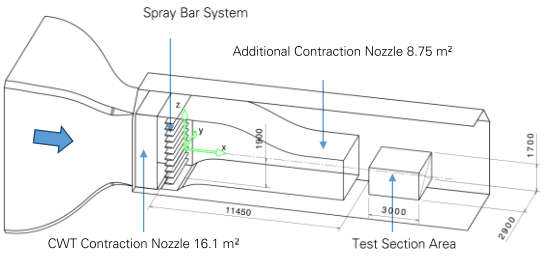

Figure 7: Test configuration with additonal contraction nozzle (8.75 m^2 cross section), as used during the KUH-1 test.

Presented at 44th European Rotorcraft Forum, Delft, The Netherlands, 19-20 September, 2018

The IWT is calibrated for the icing conditions defined in EASA CS 25/29 Appendix C and Appendix O (freezing drizzle). The achievable conditions are summarized in Table 3 below.

Icing section width / height (cross section)	3.5 m / 4.6 m (16,1m²) 3.5 m / 2.5 m (8,75 m²)
Wind speed	10 m/s to 80 m/s
LWC temperature range	-2°C to -30°C
LWC droplet size range	MVD 15 µm to 40 µm (Appendix C) MVD 20 µm to 530 µm (Appendix O)
LWC range	0,9 g/m³ (max speed) to >5 g/m³ (at min speed) for Appendix C

Table 3: Technical data IWT.

3.2. Control of the IWT and data recording

The IWT is operated by RTA in three shifts (24h, 7 days per week) from the control room using an integrated scalable-automation Facility Control System (FCS). The FCS allows the control of all IWT facility parameters (>50), as well as the recording of all controlled values and installed sensor data. In preparation for a test, the RTA test engineer is able to specify data acquisition source, type (AI, frequency, etc.), computations (temporal mean, temporal standard deviation, average of several parameters, or any Visual Basic script-compatible expressions), recording specification, descriptive information, display defaults, monitoring alarm levels, etc. The system computes the data during runtime using the sensor calibrations for each parameter. The channels and sensors calibration information / history are stored in data bases. Multiple data systems and multiple data recording sessions can coexist. The parameter properties are stored together in each recorded data file (xlsx) to ensure that the test data is traceable. All recorded data is available immediately after the test runs for further analyses.

Additionally, four permanently installed and two temporary installed cameras are recording the test section of the IWT 24h per day in HD quality. By request, up to 4 high speed cameras (up to 500 fps) can be installed.

All relevant data and video views are shown online in the measurement room (see Figure 8). This room is located close to the control room and IWT entrance door. Necessary changes in displayed data, video view, scaling of diagrams etc. can be done directly by the customers themselves. Thereby, it's possible to monitor the relevant data in real-time and compare it directly with the requirements. During the test runs the RTA test manager in charge is on the side of the customer to monitor the correct functioning of the IWT with all relevant information available. Details of the test article can be inspected at any time by remotely zooming in with the aforementioned video monitoring system equipment. Relevant test article control systems (e.g., mass flow simulation control, engine control, flap control), as well as emergency-stop controls can also be installed in the measurement room.

Figure 8: Measurement room (customer area).

3.3. IWT calibration

The evaluation and calibration of the IWT was carried out according to SAE ARP 5905 "Calibration and Acceptance of Icing Wind Tunnels". All tests required by the standard have been performed for both IWT configurations, i.e., with and without the contraction nozzle. In summary, the IWT is regularly calibrated for:

- Temperature uniformity
- Turbulence intensity
- Velocity uniformity and angularity
- MVD and LWC
- LWC uniformity

Especially the MVD and LWC measurements have been repeated in close cycles since the beginning of the RTA IWT operation in 2014. The comparison between the measured data and the curve fit is shown in Figure 9 and Figure 10. The recommended limits according the SAE ARP 5905 are shown here by the grey shading (± 10%) and dotted lines (± 20%).

Presented at 44th European Rotorcraft Forum, Delft, The Netherlands, 19-20 September, 2018

3.4. IWT LWC uniformity and LWC calibration checks for the KUH-1 test

As normal procedure before starting icing tests with the test article installed in the test section, a functionality check of the spray bar system was performed to guaranty the correct functionality of the IWT. This check included the water and air conditioning in terms of water quality and temperature control, cleanness of the spray nozzles, water flow through each nozzle, and the checking of >100 control parameters of the spray system as displayed on the FCS (plausibility check of, e.g., water/air pressure, temperatures, water conductance; broken sensors, etc.).

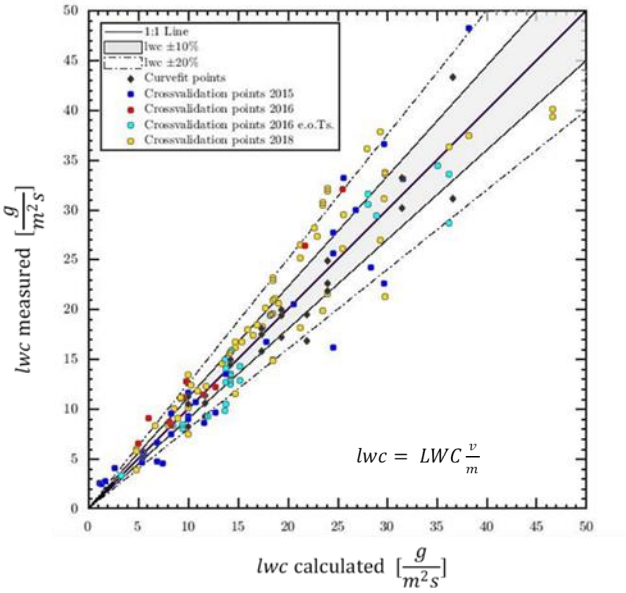

Figure 9: Comparison between measured data and the curve fit for LWC since 2014.

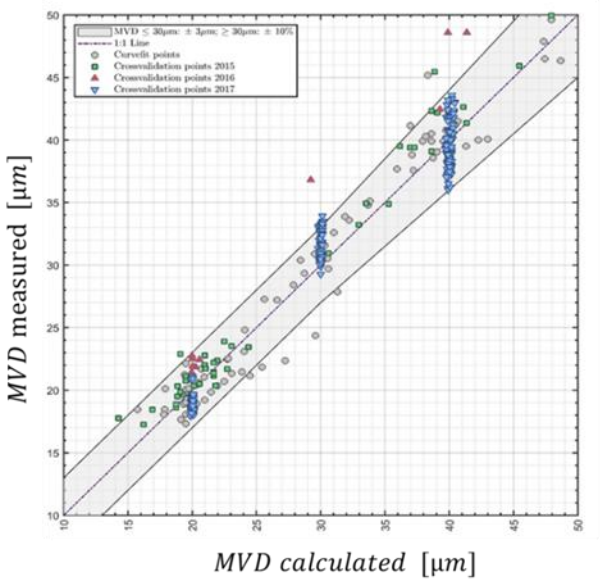

Figure 10: Comparison between measured data and the curve fit for MVD since 2014.

For certification tests, additional to the normal functional check, a calibration check of the LWC calibration and the cloud uniformity in the empty test section is typically performed. The results of the LWC measurements are compared to the curve fit of the existing calibration as shown in Figure 9. Furthermore, a standard measurement with an icing grid (see Figure 11) is performed to verify the cloud uniformity in the defined area of interest. For the KUH-1 tests, the defined area of interest was in the centreline of the IWT. The ice accumulation on the grid was measured with a calliper on every grid field after the prescribed exposure time in rime ice conditions with freezing fraction equal to unity. The ice accumulation over the grid is shown in Figure 12 for one calibration test point. The results compared favourably with previous results and the recommended requirements of the ARP 5905.

Figure 11: Grid measurement for uniformity check of the cloud condition.

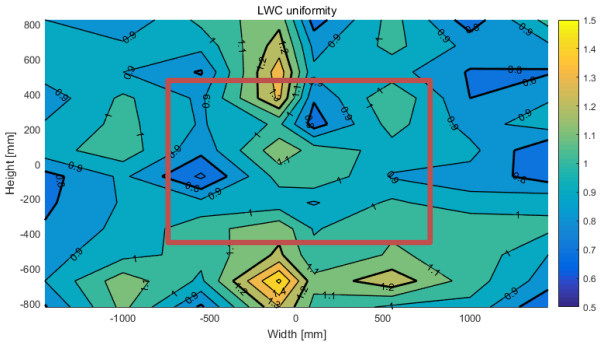

Figure 12: LWC uniformity measurement at 50 m/s with LWC 0,95 g/m³ in the empty test section.

4. WIND TUNNEL TEST

4.1. Test scope

The primary objective of the test was to obtain

Presented at 44th European Rotorcraft Forum, Delft, The Netherlands, 19-20 September, 2018

data to substantiate the compliance for the military qualification of the KUH-1 for flight in icing conditions. The Tailored Airworthiness Certification Criteria for the military qualification are based on 14 CFR Part 29, with the Appendix C envelope replaced by the icing conditions defined in DEF STAN. In light of the scheduled civil versions of the aircraft, a secondary objective of the testing was to obtain data to substantiate the engine intake anti-icing for inadvertent icing exposure in the civil 14 CFR Part 29 Appendix C envelope.

Prior to qualification testing, the first test points at RTA were aimed at reproducing flight test icing conditions, taking into account the effects of altitude, and correlating the observed ice shapes, and measured interlaminate and surface temperatures. Once a satisfactory match between the two test activities was obtained, compliance demonstration testing was initiated.

The test matrix included a static air temperature sweep to determine the critical icing temperature within the DEF STAN icing envelope. This was followed by an MVD sweep in the Appendix C envelope at the identified critical temperature. Finally, the corners of the icing envelope were also demonstrated. All DEF STAN icing test points consisted of consecutive CMI and PMI exposures. The Appendix C in-flight icing test points consisted of two cycles of consecutive standard-distance 15 minute CMI and 2.6 nm IMI exposures. The IGE hover and ground icing test points that are required by 14 CFR Part 29 were maintained for a duration of 30 minutes as specified in the regulations.

4.2. Altitude scaling

To scale for the combined effects of altitude in the sea level pressure RTA IWT, the test conditions were adjusted to match the in-flight [5]:

- Recovery temperature
- Water catch rate
- Modified inertia parameter
- Reynolds or Weber number

The Reynolds number and Weber number cannot be matched simultaneously in an unpressurized facility. Therefore, either one of the scaling parameters must be selected depending on their relevance to the system performance at a given test condition. Practically, this means that scaling was based on Weber number in warm conditions dominated by runback water/ice, and on Reynolds number in cold conditions (SAT≤-15°C) where the performance is driven by surface temperature.

In addition to the traditional scaling parameters identified above, it was necessary to adjust the sea level (SL) engine and cooling intake volume flows Q^{SL} to replicate the stagnation line position, and consequently the impingement limits, of the corresponding altitude flight condition (FL):

$$Q^{SL} = Q^{FL} \frac{U_{\infty}^{SL}}{U_{\infty}^{FL}} \tag{8}$$

Figure 13 shows the result of dedicated 3D flow and impingement analyses that were performed prior to testing to verify the scaling methodology and to quantify potential installation and open-jet effects associated with the test set-up at RTA. The peak collection efficiencies and impingement limits were matched well in the main areas of interest. The increased collection efficiency of the cooling inlets was confirmed during testing, but was not critical to the compliance of the system.

5. RESULTS

5.1. Comparison with flight test

Multiple test points at the start of the test campaign were aimed at a comparison with artificial icing flight test data obtained with the Helicopter Icing Spray System (HISS) tanker earlier in the winter season. This included comparisons in terms of ice accretion, as well as measured interlaminate and surface temperatures. The prescribed engine and cooling inlet mass flows for the wind tunnel test were estimated based on engine deck calculations.

Initial testing revealed a discrepancy in the measured temperatures compared to the flight test. This was reflected also in the duty cycle of the anti-icing system which is controlled based on an area-average of internal temperature. It was found that the discrepancy could be partly explained by the comparatively large cable distances between the model in the test section and the control units in the customer room (despite the use of thicker gauge wiring). This affected both the Voltage measured over the anti-icing heater, and the temperature measured by the anti-icing controller. The supply issue was resolved by switching to a 50 Hz variable-Voltage power supply and increasing the Voltage to achieve the nominal potential difference over the anti-icing heaters.

Presented at 44th European Rotorcraft Forum, Delft, The Netherlands, 19-20 September, 2018

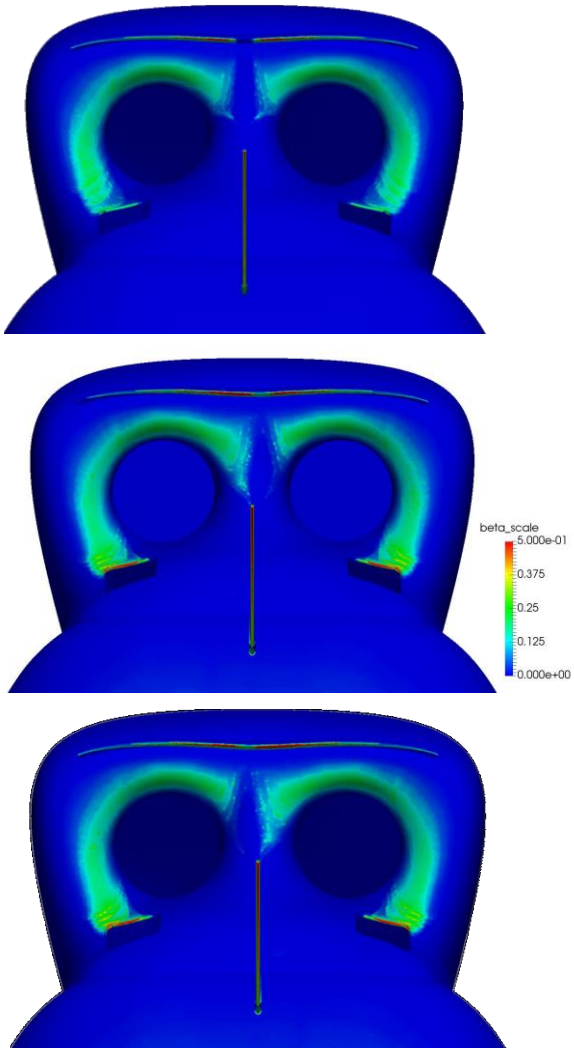

Figure 13: Comparison of predicted drop collection efficiency in free-flight at 10,000 ft pressure altitude (top), and in Weber (middle) and Reynolds number (bottom) scaled sea level test conditions inside RTA test section. Courtesy: AeroTex UK.

After the corrections to the power supply, a detailed review of the surface temperatures revealed a residual discrepancy in the dry air stabilized heat-off temperatures, as well as in the rise time. Whereas the heat-off surface temperatures measured in the wind tunnel were close to the expected total temperature, the flight test data from the same location showed a 5°C increment above the static air temperature. It was concluded that, on the test aircraft, the components aft of the engine inlet constituted a non-negligible heat source. To simulate this additional heat source, a hot-air blower was installed inside the inlet cowling and the fan speed was adjusted at constant heater power to achieve the desired temperature increment. The net result was a better correlation with flight test while retaining some conservatism.

Figure 14 shows the final comparison between the Reynolds-scaled wind tunnel test and the artificial icing flight test in terms of inlet ice accretion. The wind tunnel ice shapes are observed to be larger than during the flight test, but still well within the engine ice ingestion limits. The conservatism of the wind tunnel test set up is attributed to:

- Lower measured surface temperature due to residual RTD measurement bias associated with long leads to controller in customer room.
- Reduced aerodynamic ice shedding forces due to Reynolds number airspeed scaling.
- Non-uniformity of icing spray LWC at the height of the cooling inlets.
- Local ice accretion on instrumentation wiring.

In prior NLR-KAI icing wind tunnel testing of a 2D section of the intake at Cox & Co, the surface thermocouples were imbedded inside the top rubber layer of the heater mat. Due to the complexity of the geometry, this was not possible on the 3D production part. The thermocouple wiring was, therefore, secured using aluminium tape, leading to local cold spots on the surface of the intake. Part of the thermocouples was removed during subsequent test points in favour of obtaining a more representative surface temperature distribution.

5.2. Critical icing conditions

The critical icing conditions for a given system may be hard to define under the combined influence of static air temperature, liquid water content, drop size and flight condition. In the case of the KUH-1, the qualification focused on high-speed cruise without cloud extent scaling, with emphasis on ice accreting on areas of the intake where engine ingestion was considered possible (in any post-icing flight condition).

To determine the critical icing conditions, a static air temperature sweep was performed at DEF STAN CMI LWC and 20 µm MVD (equivalent to Appendix C CMI at 15 µm). A critical evaluation of the relevant ice masses and surface temperatures revealed the critical static air temperature to lie between -15°C and -20°C. This condition balances the higher convective heat loss of increasingly colder temperatures with the decreasing maximum liquid water available at colder temperatures in the certification envelopes. A subsequent MVD sweep from 15 µm to 40 µm in the Appendix C envelope at the identified critical temperature showed that 20 µm was in fact the critical MVD.

Presented at 44th European Rotorcraft Forum, Delft, The Netherlands, 19-20 September, 2018

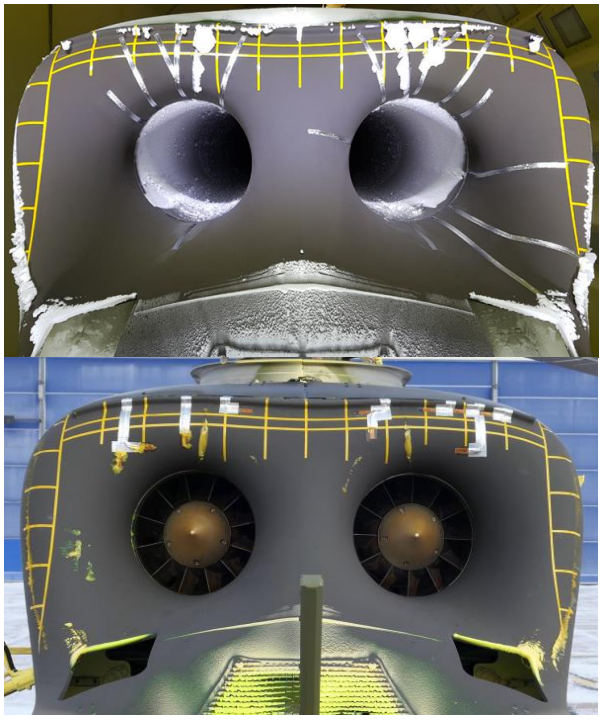

Figure 14: Ice accretion comparison between artificial icing flight test (top) and icing wind tunnel test (below). Reynolds-scaled test conditions at -20°C static air temperature. The yellow ice accretion on the artificial icing flight test is the result of food dye added to the spray water.

5.3. 3D ice accretion scans

Due to the complex geometry of some of the parts of the KUH-1 engine intake and the related ice shapes, traditional cross-section tracing of ice accreting on the intake is difficult and does not yield a great deal of information. Moreover, since the intake is not an aerodynamic lifting surface, the emphasis here is on ice volume/mass rather than on the shape of the cross-section. To obtain volumetric information of the accreted ice shapes, 3-D scans were generated for a selected number of test runs. The scanning and related processing was performed by the Austrian Institute for Icing Sciences (AIIS).

An example scan is provided in Figure 15 which shows ice accreted on the left-hand engine cooling inlet. Besides forming a basis for validation of ice accretion predictions, the scans were also useful in generating a post-test breakdown of ice mass where scale measurements were not available. Note that the extent of ice accretion in Figure 15 is influenced by the aluminium tape used to secure the thermocouples.

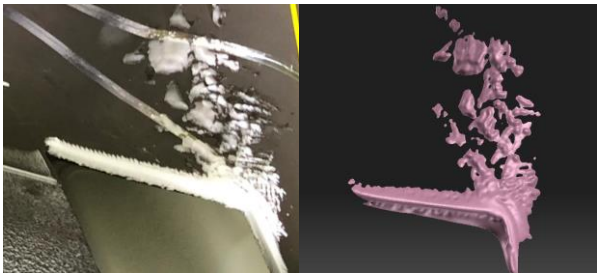

Figure 15: 3-D scan of ice accreted on left-hand engine cooling inlet.

6. CONCLUSION

An extensive icing qualification wind tunnel test campaign was performed to substantiate the compliance of the KUH-1 engine air intake for the military qualification for flight in icing conditions. The intake was tested at full-scale with the production anti-icing system and aspirated using the purpose-built Engine Mass Flow Simulator (EMFS). The EMFS provided stable mass flow control for the main and cooling inlets separately.

The correlation with icing flight test data revealed a conservative discrepancy in test surface temperatures due to the absence of engine heat sources and controller temperature sensor bias. The ice accretions observed in the IWT were exaggerated by surface temperature instrumentation, non-uniformities in icing spray LWC, and due to a reduction in aerodynamic shedding forces in Reynolds-scaled test conditions. Despite the conservative nature of the test, compliance with the regulatory requirements was successfully demonstrated. The KUH-1 has since been awarded military qualification for flight in icing conditions.

7. ACKNOWLEDGEMENTS

The authors would like to acknowledge Dave Parkins and the KAI test team consisting of Kihyun Kim and Hyung Sik Kim for their teamwork during the test.

8. REFERENCES

[1] S.C. van ‘t Hoff, J. van der Vorst, R.J. Flemming, and D.C. Parkins, “Icing Certification of Korean Utility Helicopter KUH-1: Artificial Icing Flight Test”, presented at the AIAA Aviation Forum 2017, Denver, Colorado, June 5-9, 2017.

[2] De Bruin, A. C., Fatigani, G. and Shin, H. B., “KAI Surion Helicopter Full-Scale Air Intake

Presented at 44th European Rotorcraft Forum, Delft, The Netherlands, 19-20 September, 2018

Testing at CIRA Icing Wind Tunnel," presented at 30th Congress of International Council of the Aeronautical Sciences, Daejeon, Korea, September 25-30, 2016.

[3] ISO/TC 30/SC 2, "Measurement of Fluid Flow by Means of Pressure Differential Devices Inserted in Circular Cross Section Conduits Running Full - Part 2: Orifice Plates", EN ISO, 5167-2, 2003.

[4] H. Schlichting et al, "Boundary-layer theory (Vol. 7)", McGraw-Hill, New York, 1995.

[5] D.N. Anderson, "Manual of Scaling Methods", NASA/CR-2004-212875, March, 2004.

[6] B. Bauer and F. Galavics, "Experimentelle und theoretische Untersuchungen über die Rohrreibung von Heizwasserleitungen", Fernheizkraftwerkes d. ETH, Zürich, 1936.

[7] Nikuradse, J., "Strömungsgesetze in rauhen Rohren", Forschg. Arb. Ing.-Wes. No. 361, 1933.

Presented at 44th European Rotorcraft Forum, Delft, The Netherlands, 19-20 September, 2018